Available online at www.sciencedirect.com
SCIENCE DIRECT®
Estuarine, Coastal and Shelf Science 59 (2004) 33–47
ESTUARINE COASTAL AND SHELF SCIENCE

Short-term dynamics and maintenance processes of headland-associated sandbanks: Shambles Bank, English Channel, UK

A.C. Bastos*, D. Paphitis, M.B. Collins

School of Ocean and Earth Science, University of Southampton, Southampton Oceanography Centre, European Way, Southampton SO14 3ZH, UK

Received 6 June 2002; accepted 25 July 2003

Abstract

The short-term (over a spring tidal cycle) dynamics of a headland-associated sandbank (Shambles Bank, English Channel) are investigated, by means of field measurements (synchronous data, using an acoustic Doppler current profiler (ADCP) and repeated side-scan sonar imagery) and two-dimensional (2D) hydrodynamic and sediment transport models. The dynamics of the bank are described in terms of along- and cross-bank velocity components, sand transport pathways and bedform asymmetries.

The results showed the occurrence of a net bedload convergent zone along the crest of the bank as a result of anti-clockwise veering of sediment transport towards the crest. This transport pattern is suggested to be the result of the dynamic interplay between two distinct tidally related processes acting over the sandbank, during each phase of the tidal cycle: (a) the formation and different stages of a transient tidal eddy that drives bedload movement during the flood phase of the tide and (b) the bottom-friction induced by the presence of the sandbank that governs the bedload transport dynamics during the ebb phase of the tidal cycle.

Keywords: headland-associated sandbanks; bedform asymmetry; bedload transport; tidal (transient) eddies

1. Background

Sandbanks are present on tidally and wave-dominated continental shelves and within coastal and estuarine environments; they are, generally, the result of abundant sediment availability and strong currents capable of inducing bedload movement. The formation of a sandbank is associated with the accumulation of sand; this, in fact, is a response to regional sediment transport patterns and gradients in the transport rates. Sand accumulation is likely to occur due to bedload convergence, or a decrease in the bed shear stress along the transport pathway. Once formed, sandbanks develop and are being maintained through the continued (dynamic) interaction with the hydrodynamics. Different types of banks have been described elsewhere, in relation to their morphology, regional setting and formation and maintenance processes (for reviews see, Pattiaratchi and Collins (1987) and Dyer and Huntley (1999)).

There have been many studies attempting to classify sandbanks. Off (1963) described rhythmic linear sand bodies caused by currents, based up on world-wide occurrences. Swift (1975) distinguished, in addition to sandbanks occurring on shelf edges, two different types based upon Off's description: estuarine or embayment ridges (parallel to the axis of the embayment or estuary) and ridges, off capes and promontories (coast-parallel, tending to be elongated normal to the shore). Pattiaratchi and Collins (1987) described seven different categories of sandbanks, based upon the orientation of the adjacent coastline and to the direction of the prevailing currents. Subsequently, in an extensive review on sandbank classification, Dyer and Huntley (1999) suggested a generic classification based upon their formation and development. These investigators pointed out the necessity to distinguish between the regional

* Corresponding author.
E-mail address: acb4@soc.soton.ac.uk (A.C. Bastos).

0272-7714/03/$ - see front matter © 2003 Elsevier Ltd. All rights reserved.
doi:10.1016/j.ecss.2003.07.008

context of banks, in terms of their geological origin, and the localised and short-term hydrodynamic processes acting towards its development and maintenance. Three different types of sandbanks were proposed: open shelf ridges (Type 1); estuary mouth banks (Type 2, ridges and tidal deltas); and headland-associated banks (Type 3, banner banks and alternating ridges).

There have also been many studies proposing mechanisms for sandbank formation and maintenance, such as: the spiral flow concept (Houbolt, 1968); the bed shear stress stability model (Smith, 1969); the tidal stirring concept (Pingree, 1978); response to standing edge waves (Dolan et al., 1979); and the seabed stability model (Huthnance, 1982a,b). Given the aims of the present investigation the mechanisms proposed by Pingree (1978) and Huthnance (1982a,b) are considered below in somewhat greater detail. Huthnance (1982a,b) explained the formation of sandbanks as being the result of instabilities on the seabed, in response to interaction between the seabed topography, tidal currents and sediment transport. The stability model (followed, subsequently, by other authors such as: de Vriend, 1990; Hulscher et al., 1993; Trowbridge, 1995; Hulscher, 1996; Calvete et al., 2001; Hulscher and van den Brink, 2001) explains the growth of a sandbank lying obliquely to the tidal current direction, by describing the pattern of cross- and along-bank components of the flow. As the tidal flow approaches the bank the along-bank component of velocity decreases (due to an increased bottom-friction) whereas the cross-bank component (by continuity) increases, resulting in the flow veering towards the crest of the bank. Consequently, sand is transported towards the crest of the bank and with the reversal of the tides there is a convergence of sand along the crest. This concept is supported by the observed morphology of linear sandbanks elsewhere (e.g. Caston, 1972; Kenyon et al., 1981; Belderson et al., 1982; Lanckneus and de Moor, 1995).

The formation of headland-associated sandbanks (Type 3, according to Dyer and Huntley, 1999), could be explained by the convergence of secondary flows associated with residual eddies (the tidal stirring concept, introduced by Pingree (1978)) and/or the convergence of sand transport induced by transient eddies (Signell and Harris, 2000; Bastos et al., 2002). The tidal stirring concept attempts to explain the formation of sandbanks in the centre of residual eddies, generated by coastal irregularities (e.g. headlands, Tee, 1976; Pingree, 1978; Ferentinos and Collins, 1980). The idea is that these eddies generate secondary flows that converge towards the centre of the eddy at the seabed and, by continuity, diverge at the surface. This pattern is controlled by the balance between the pressure gradient, inertial forces (bottom-friction) and planetary vorticity. A low pressure region at the centre of the eddy leads to a flow convergence at the seabed; this, consequently, gives rise to sand accumulation. However, the major limitations to the application of this concept are: (a) that secondary flows represent only around 5–15% of the overall flow and (b) residual flows can be an order of magnitude lower than the instantaneous flow patterns (Heathershaw and Hammond, 1980; Geyer, 1993). These observations can be important in terms of sediment transport, in cases where the critical shear stress required for the initiation of sediment movement is not reached (Dyer and Huntley, 1999; Bastos et al., 2002). In addition, it would be relevant to point out that the tidal stirring concept predicts the formation of asymmetric sandbanks around headlands due to the effect of the Earth's rotation. This is conceivable where planetary and residual vorticity are comparable (as argued by Pingree, 1978 for the banks around Portland Bill, southern UK); in this case, the residual bottom flows will act differently (converge and diverge, respectively) on either side of the headland. However, for an idealised situation, Signell and Harris (2000) showed that changing the sign of the Earth's rotation (planetary vorticity) had no significant effect on sandbank formation, i.e. the residual stirring of the tidal currents could not explain the formation of headland-associated sandbanks. These authors suggested that transient patterns in shear stress and sediment flux are more relevant for this type of sandbanks.

The present study examines the tidally induced short-term (ebb-flood spring tidal cycle) hydrodynamics and sediment (including bedform) dynamics associated with the tidally related maintenance processes of the Shambles Bank (English Channel, Fig. 1). Towards this objective, current measurements (with an acoustic Doppler current profiler (ADCP)) and side-scan sonar data (obtained synchronously) are used in combination with two-dimensional (2D) hydrodynamic and sand transport models.

2. Environmental setting

The Shambles Bank (Fig. 1) is an elliptically shaped bank lying on top of a flat bedrock erosional surface, with a maximum height of 22 m above the surrounding seabed, which lies at 30 m (Bastos et al., 2002); it is about 5 km long and 2 km wide. The bank is aligned in an NE–SW direction, sub-parallel to the eastern coast of the Isle of Portland; it shows a strongly asymmetric profile, being steeper towards the coast (NW). The bank is characterised by the occurrence of very large sandwaves (wavelength of 300 m and maximum crest heights of 7 m), with medium and smaller size sandwaves superimposed upon the flanks and/or along the troughs. These small- and medium-sized sandwaves form usually an oblique angle with the major sandwave crest. A convergent zone of sand transport is indicated

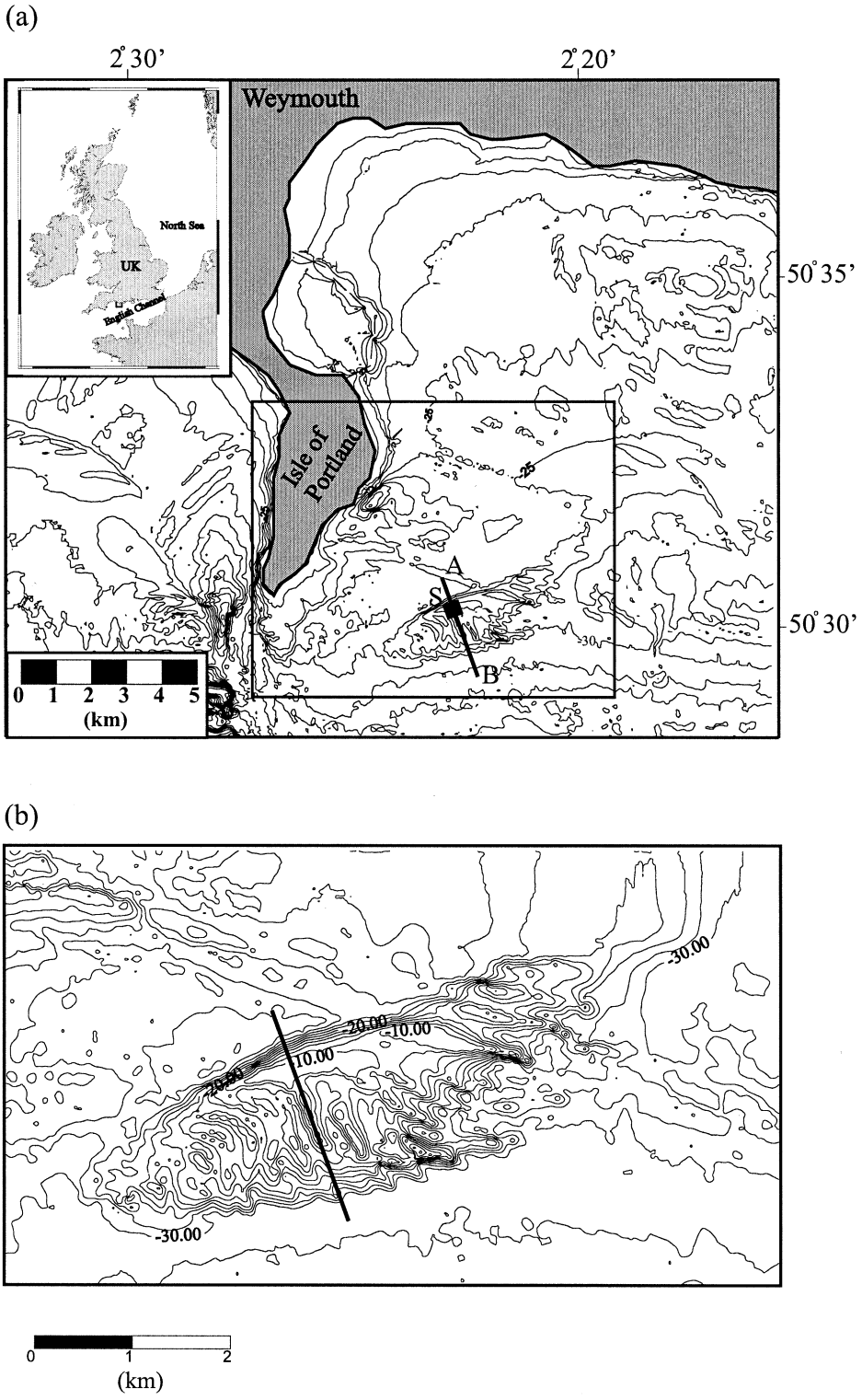

Fig. 1. Location of the area under investigation: (a) regional setting of the Shambles Bank along the southern coast of the UK (line A–B is the survey transect and the box marks the selected side-scan sonar survey area) and (b) detailed bathymetry of the Shambles Bank. Bathymetry in metres (relative to Chart Datum).

by the asymmetry of these large sandwaves. Flood-dominated asymmetric profiles (pointing towards the NE) are observed along the southwestern flank, whereas the northeastern flank is characterised by the presence of ebb-dominated asymmetric profiles (pointing towards the SW). In terms of sediment composition, the Shambles Bank is characterised, predominantly, by bioclastic material (70%–80%, by weight) ranging

from coarse sand ($D_{50} = 0.9$ mm) to sandy-gravel size ($D_{50} = 2.4$ mm); cohesionless quartz grains represent the remainder of samples. The carbonate content was identified (on the basis of qualitative analysis) as shell fragments of the mussel *Mytilus edulis* ($\rho_s = 2.72$ g cm^{-3}). The mean grain size was found to decrease, towards the southwestern end of the bank.

3. Methods

3.1. Field survey

A fieldwork programme was designed to provide synchronous information on the prevailing hydrodynamics and the associated seabed response, throughout a complete tidal cycle (13 h, during the peak of spring tides, in July 2001) across the Shambles Bank (Fig. 1). The survey was undertaken under mild meteorological conditions, with wind speeds below 3 m s^{-1}; this resulted in an insignificant wave action superimposed upon the prevailing tidal currents. The experiment consisted of repeated 3.75 km cross-bank transects (line A–B, Fig. 1). Each was completed within a 30 min period using a ship-mounted ADCP (600 Hz, with a vertical resolution of 2 m and depth range of 47 m) and high-resolution side-scan sonar (GeoAcoustic, 500 kHz). Navigational data were acquired using a differential geographical positioning system (DGPS), precise to within ± 1 m.

The first of the velocity measurements acquired by the ADCP was about 1.5 m below the water surface (herein referred to as 'surface currents'), whereas the deepest measurement was about 1.5 m above the seabed (herein referred to as 'near-bed currents'). The instrument transmitted averaged data, to an on-board PC, once every 5 s; these were processed and averaged to a horizontal sampling interval of 50 m (or a time interval of 20 s for a boat speed of 2.5 m s^{-1}). Given the main orientation of the sandbank (major axis orientated at 70°–250° and the survey transect 340°–160°) the data were transformed into along-bank (parallel, x-component positive to the NE) and cross-bank (perpendicular, y-component positive to the NW) velocity components.

Seabed imagery was acquired simultaneously with the ADCP current data, using side-scan sonar (50 m range on either side); these transects formed a time-series and were analysed individually. The data were used to investigate changes (orientation and asymmetry) in the small-scale bedforms (small to medium sandwaves, according to Ashley, 1990). A specific area along the bank crest (about 250 m long) was selected to represent the observed bedform changes (Fig. 1). The mean water depth at the selected site was 10 m, with an associated mean grain size of 1.1 mm (75% carbonate content).

3.2. Numerical modelling

3.2.1. Hydrodynamic model

Tidal flow patterns were characterised over the study area using the results derived from a depth-averaged hydrodynamic model (TELEMAC-2D), which had been already set up and calibrated for the area under investigation (Brampton et al., 1998). It has to be pointed out that the model was set up originally for the investigation of the tidal flow patterns along the Dorset continental shelf, covering an area of approximately 7500 km^2. As such, the model results presented here are intended to provide a regional perspective of the hydrodynamics and sediment dynamics on the eastern side of Portland Bill and in the vicinity of the Shambles Bank.

TELEMAC-2D is a finite element model, based upon shallow-water equations that describe the conservation of water mass and momentum (Hervouet, 1991). The model uses an irregular grid of triangular elements, allowing areas of special interest to be examined in greater detail. Output files containing tidal current and water-level data (for spring and neap tides) were processed (over the whole tidal cycle and for every grid point), in relation to vorticity (calculated at each time-step), residual currents (calculated by averaging the depth-averaged current) and the maximum and mean current velocities.

3.2.2. Sediment transport model

Bedload transport was computed using a sediment transport model (SEDTRANS), which calculates bottom shear stresses (under currents alone and combined flows) and sediment transport rates for a given input dataset of: water depth; current speed and direction; wave height and period; bed roughness; and grain size (for further details see Li and Amos, 1995). For the present study, the 'potential' bedload transport rates were calculated using the algorithm proposed by Gadd et al. (1978). This selection was based upon the results obtained by Grochowski et al. (1993), who found reasonable agreement between the predicted and observed (using radioactive tracers along the French coastline, see Dewez et al., 1989) bedload transport rates within the English Channel. Transport simulations were carried out using the mean grain size (D_{50}) distribution, established over the study area. Critical shear velocities were calculated using Yalin (1977), which have been shown to be in reasonable agreement with laboratory results concerning bioclastic sands (Paphitis et al., 2002). Along the survey transect, the measured (ADCP) velocities were used for the computation of bedload transport; for the remainder of the study area, the computed (hydrodynamic model) velocities were used.

4. Results

4.1. Hydrodynamics

The results obtained from the ADCP measurements show distinct current patterns over the Shambles Bank, associated with the ebb and flood phases of the tidal cycle. The patterns relate to the spatial distribution of the along- and cross-bank flow components. The depth-averaged velocities computed by the hydrodynamic model are plotted in the background, together with the ADCP results (Figs. 2–4), to establish a more complete picture of the prevailing hydrodynamics over the study area.

During the flood phase (about 3 h after slack water), the currents are flowing towards the E–NE; they are affected by the presence of the headland (Fig. 2). Along the bank (Fig. 2a), strong currents occur generally offshore (~2.00 m s^{-1}) of the southern flank; these

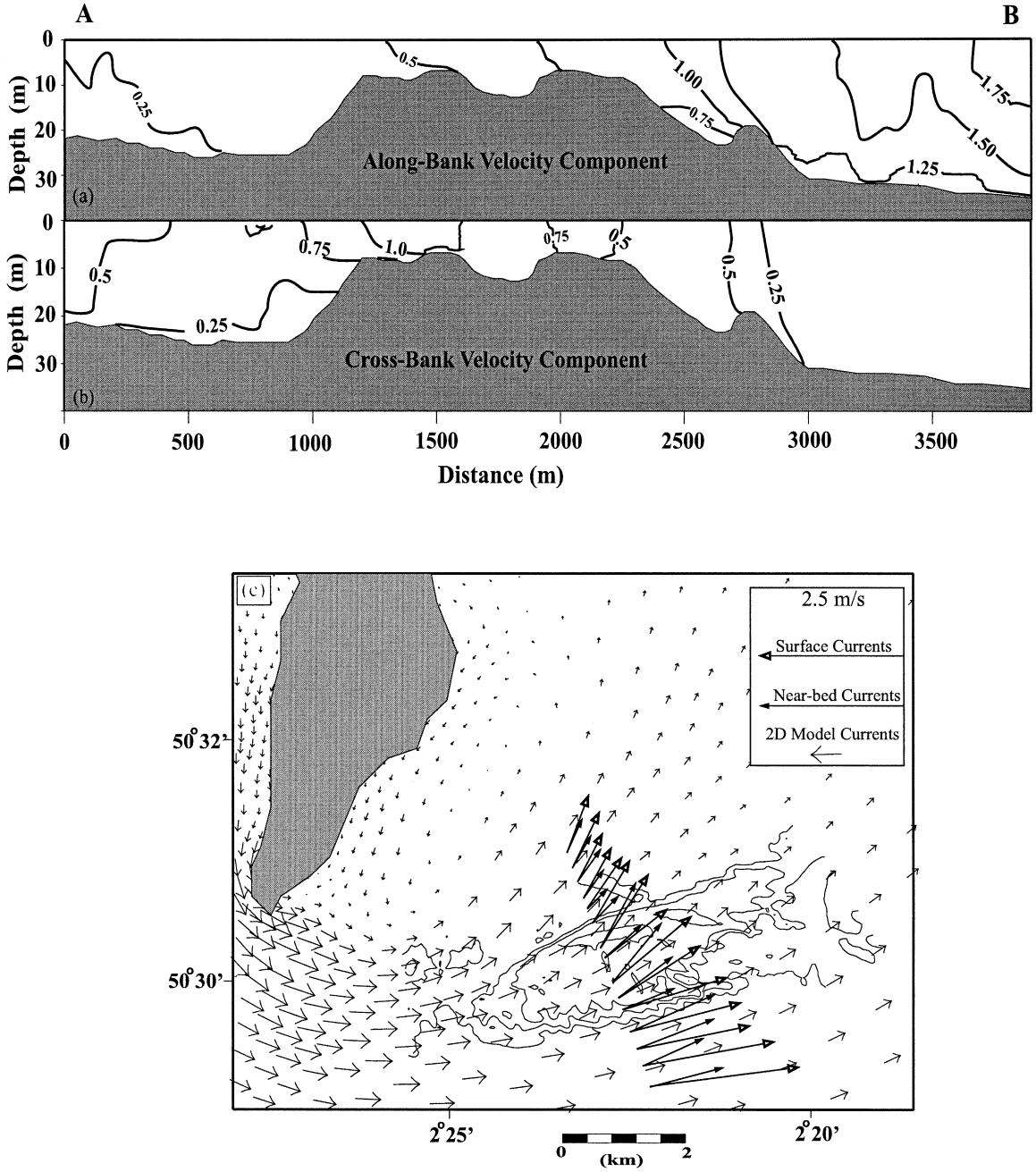

Fig. 2. Flow pattern obtained from the ADCP results, during the maximum flood currents: (a) the along-bank current component (m/s; positive *x*-axis toward the NE); (b) cross-bank current component (m/s; positive *y*-axis toward the NW); and (c) surface (open arrows) and near-bed (black arrows) tidal current vectors, together with the depth-averaged velocities, as computed by the numerical model. Note: scale differences between the ADCP arrows and the numerical model arrows.

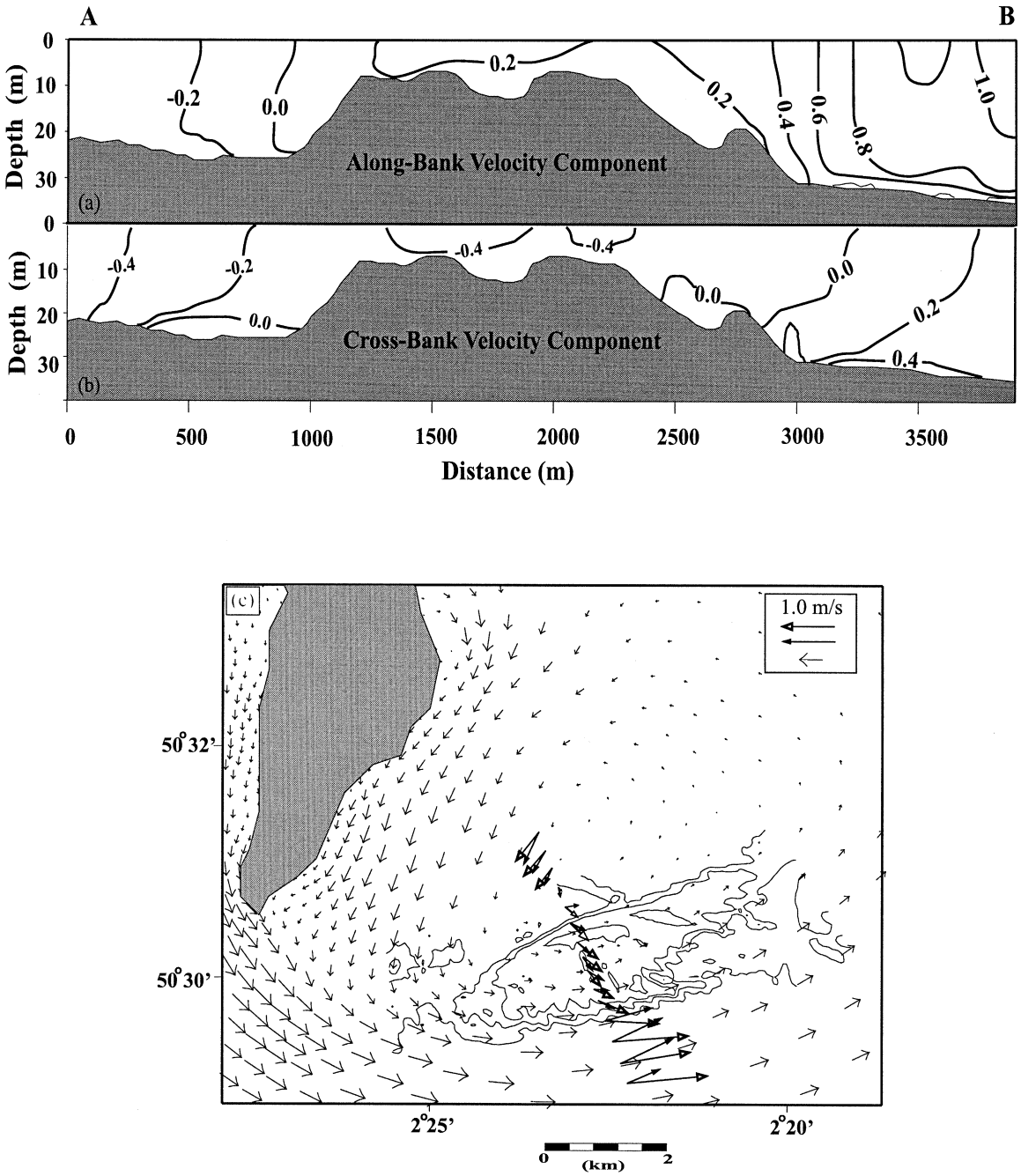

Fig. 3. Flow pattern obtained from the ADCP results, during the time-step at which the centre of the transient eddy lies over the Shambles Bank: (a) along-bank current component (m/s; positive x-axis toward the NE); (b) cross-bank velocity current (m/s; positive y-axis toward the NW); and (c) surface (open arrows) and near-bed (black arrows) tidal current vectors, together with the depth-averaged velocities, as computed by the numerical model. Note: scale differences between the ADCP arrows and the numerical model arrows.

reduce significantly as the flow approaches the bank crest (down to $\sim$0.30 m s^{-1}). This is followed by an increase in the cross-bank velocity component (from 0.20 m s^{-1} to 1.00 m s^{-1}), which causes the flow to veer towards the crest of the bank (Fig. 2b). Flow acceleration is observed, locally, at the crest of the large bedforms. Overall, water circulation during the flood induces an anti-clockwise veering of the tidal currents, towards the bank crest, which is associated with the development of a tidal (transient) eddy (clearly visible between the bank and the headland). Tidal current veering is observed throughout the entire water column; however, it is more pronounced in the near-bed currents than in the surface currents (Fig. 2c). As the flow leaves the bank crest over its northern flank, a continuous and significant decrease in the along-bank velocity component is followed by a small decrease in the cross-bank component.

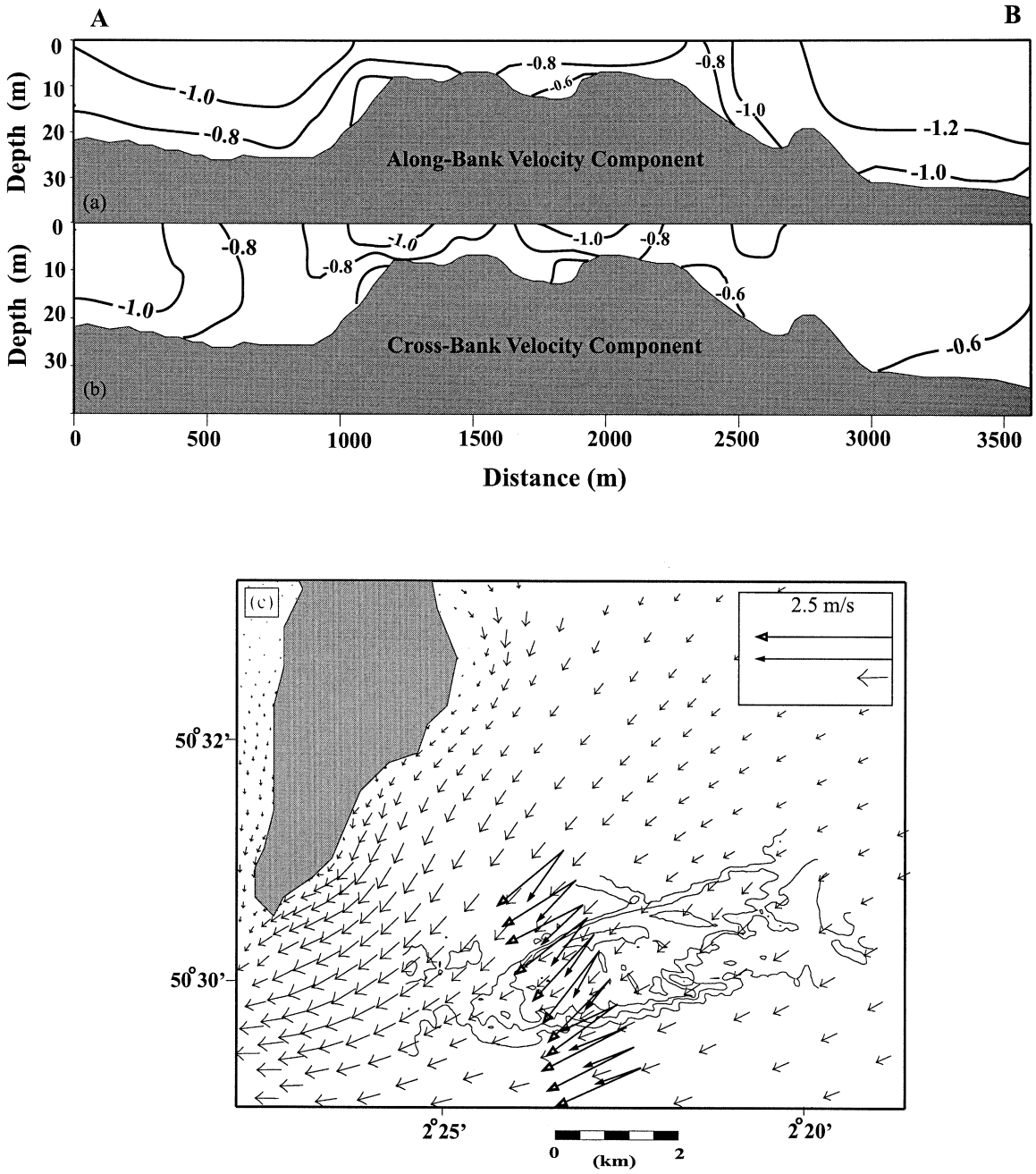

Fig. 4. Flow pattern obtained from the ADCP results, during the maximum ebb currents: (a) along-bank current component (m/s; positive x-axis toward the NE); (b) cross-bank velocity current (m/s; positive y-axis toward the NW); and (c) surface (open arrows) and near-bed (black arrows) tidal current vectors, together with the depth-averaged velocities, as computed by the numerical model. Note: scale differences between the ADCP arrows and the numerical model arrows.

In Fig. 3, the time-step at which the centre of the eddy was detected along the survey transect (about 6 h into the flood phase, close to slack water) is presented. The along-bank velocity component shows a general reduction, down to 1.25 m s^{-1} offshore (on the southern flank of the bank) and 0.20 m s^{-1} at the crest (Fig. 3a), together with a reversal in the direction (westward flow) observed towards the northern flank. The cross-bank velocity component decreases (down to zero) as the (northward) flow approaches the southern flank of the bank from offshore (Fig. 3b); here it reverses to a southward flow. The observed changes in the current direction are influenced, primarily, by the development of the transient eddy, whose presence is supported by the measured and computed velocity pattern over the area (Fig. 3c).

With the tidal reversal, the ebbing currents flow towards the SW (generally, with a direction of 230°), following the coastline contour. The time-step within the

tidal cycle, at which the ebb flow is at its maximum (about 3 h after slack water), is shown in Fig. 4. Along the survey transect, a decrease in the overall flow is observed towards the bank crest, as the contours tend to follow the topography. The current speeds reach up to 1.65 m s^{-1} (inshore) to the north, 0.90 m s^{-1} at the bank crest and 1.60 m s^{-1} (offshore) to the south (Fig. 4a). The cross-bank velocity component shows a slight increase towards the crest, as the flow approaches the bank obliquely from the N–NE (Fig. 4b). However, as the flow leaves the bank along the southern flank, the decrease in the cross-bank component is followed by a significant increase in the along-bank velocity component (Fig. 4a). The presence of the bank induces an anti-clockwise veering of the tidal currents, towards the crest, as the flow approaches the bank obliquely from the NE. Similarly, a clockwise veering is induced as the flow leaves the crest of the bank, at the southern flank (Fig. 4c); this pattern is observed throughout the entire water column.

4.2. Bedload sediment transport

The derived bedload transport rates, computed using the methodology described previously, are shown in Fig. 5. During the flood phase of the tide, sand transport was predicted to be significantly high (1.8 kg m^{-1} s^{-1} at maximum flood currents), towards the E–NE, just offshore from the southern flank of the bank. Towards the bank crest, a decrease in the transport rates was predicted, ranging between 0.07 kg m^{-1} s^{-1} and 0.80 kg m^{-1} s^{-1}; this is followed by a slight anti-clockwise veering in the sand transport direction (Fig. 5a). The steady decrease in the flow (as it leaves the bank) over the northern flank (observed previously, see Fig. 2) is followed by a significant reduction in the sand transport rates. When the core of the transient eddy was positioned over the survey transect (close to slack water, see Fig. 3), no sand movement is predicted along the bank crest. There is only a very low transport rate predicted towards the SW, at the northern end of the transect (0.009 kg m^{-1} s^{-1}) (Fig. 5b). Higher rates are predicted towards the NE, just offshore of the southern flank of the bank (of up to 0.25 kg m^{-1} s^{-1}). During the above two time-steps (Fig. 5a and b) the flow pattern and, in turn, the bedload transport rates are influenced by the presence of the headland and the different stages of the transient eddy. The flood-associated bedload sediment transport is characterised by an anti-clockwise veering towards the crest, from the southern flank; this is followed by a decrease in the transport rates at the crest.

In contrast to the flood phase of the tidal cycle, the ebbing flows induce a significant level of sediment movement throughout the entire system, with a notable reduction towards the crest of the bank. At maximum ebb currents (Fig. 5), the rates vary from 0.7 kg m^{-1} s^{-1} (along the crest) to 1.5 kg m^{-1} s^{-1} (at the northern flank). The sediment movement is associated with an anti-clockwise veering (towards the crest) (Fig. 5c). Along the crest, the rates were shown to reduce within the troughs

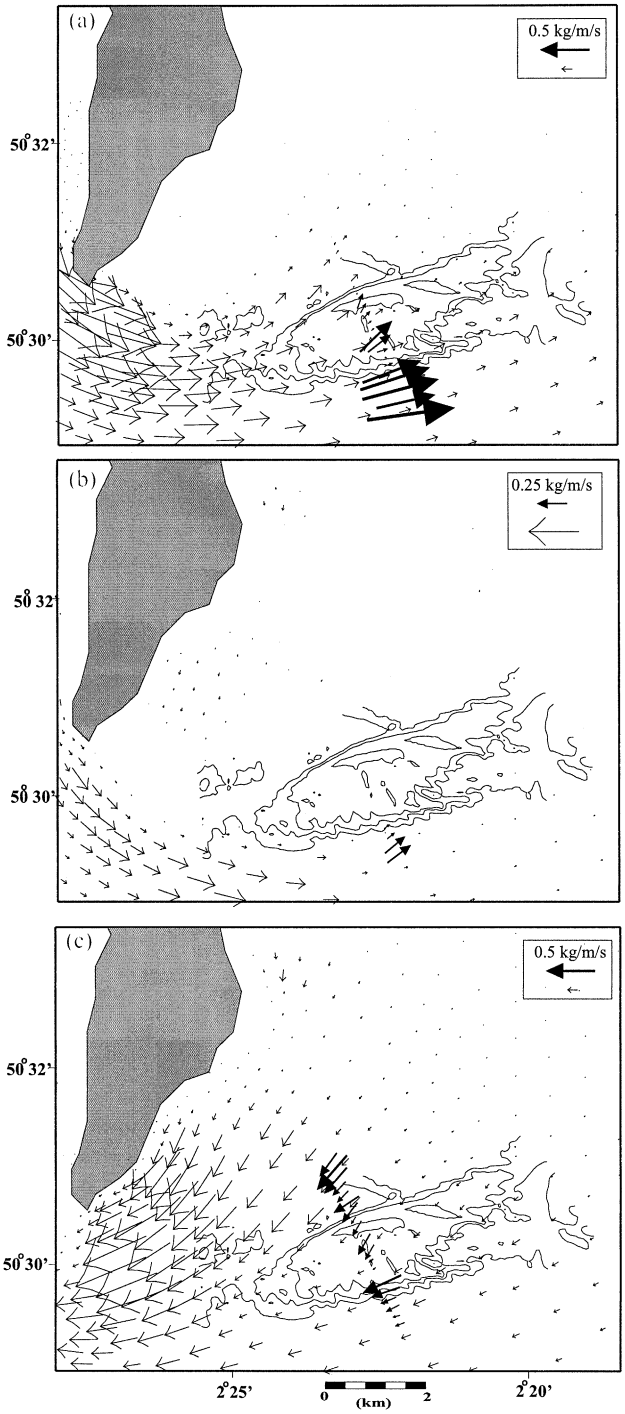

Fig. 5. Instantaneous bedload (sand) transport vectors predicted during: (a) maximum flood (Fig. 3); (b) a transient eddy over the bank (Fig. 4); and (c) maximum ebb (Fig. 5). The ADCP results were used for the survey transect whereas, for the remainder of the area, the model results (®) were utilised. Note: scale differences between the arrows showing the rates calculated using ADCP and numerical model results.

of the larger bedforms. Along the southern flank, where the flow leaves the bank, the sand transport rates are increased significantly (reaching 1.4 kg m^{-1} s^{-1}) and the pathways veer in a clockwise direction. The bedload sediment transport, associated with the ebb phase of the tide, is characterised by an anti-clockwise veering towards the crest from the northern flank; this is followed by a decrease in the predicted transport rates, at the crest.

The resultant sand transport pattern over the complete tidal cycle is characterised by an anti-clockwise circulation around the bank, followed by a decrease in transport rates towards the crest. The computed short-term bedload transport rates and directions, derived from the near-bed ADCP measurements and from the depth-averaged model, show the occurrence of a sand convergent zone along the crest of the bank (Fig. 6). A comparison between the derived residual (over a tidal cycle) bedload transport rates using ADCP measurements and the 2D hydrodynamic model results is shown in Fig. 7. The plots reveal that both datasets provide a similar general pattern of bedload transport rates and direction across the bank (Fig. 7a and b). This pattern is characterised by sediment convergence towards the crest of the bank (Fig. 7b and c), followed by a decrease in transport rates (Fig. 7a). This can be used as an indication of sediment deposition along the bank crest. However, differences can be observed regarding the absolute values of bedload transport rates as derived from the ADCP measurements and the 2D hydrodynamic model, despite the utilisation of the same sand transport model (SEDTRANS) for the computations. The observed differences are the result of: (a) the vertical resolution relating to the detailed three-dimensional (3D) structure of the flow, as resolved by the ADCP and (b) the horizontal resolution regarding the more accurate representation of the morphology of the bank, as sampled by the ADCP.

Bedload transport computations were not undertaken under the influence of superimposed waves, given their absence at the time of the survey. However, waves can contribute towards the maintenance of sandbank, particularly under storm conditions. Several researchers have highlighted the importance of storm waves in the evolution and migration of sedimentary deposits (Ferentinos and Collins, 1980; Houthuy and De Wolf, 1994; Berne et al., 1994; Tessier et al., 1999). Under storm conditions, the bank crest is reworked by wave action, which controls the height of the sandbank.

4.3. Bedform dynamics

The seabed imagery time-series has revealed reversal in the asymmetry of the small sandwaves (SSW), lying along the bank crest; these have an average wavelength of 3 m and an average height of 0.65 m. Bedform reversal was observed on the basis of the backscatter response of the profiles (whereby low tonality is related to low backscatter). The SSW crestlines over the selected

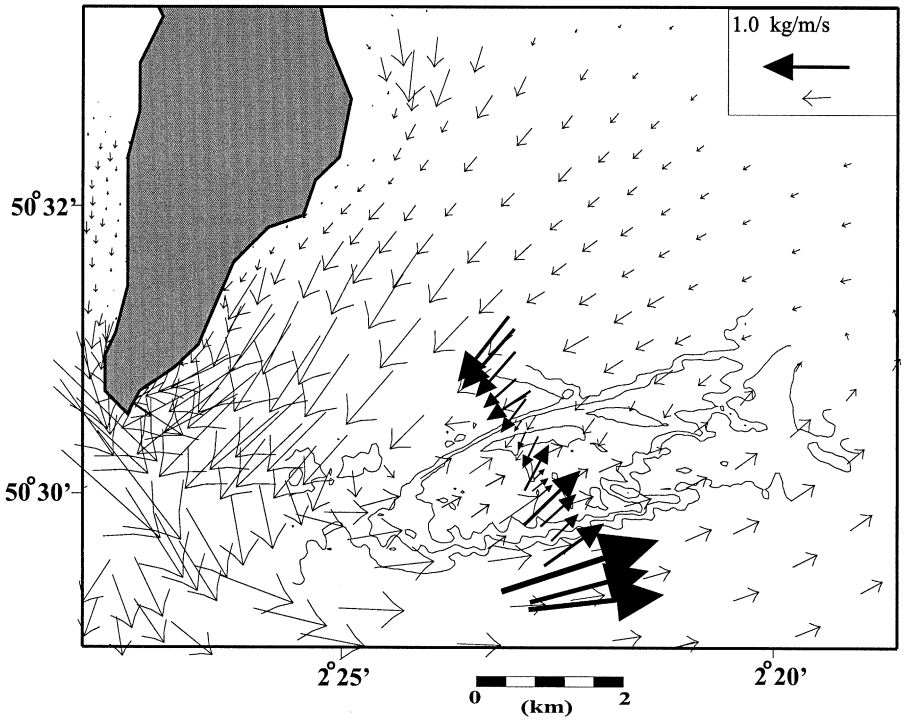

Fig. 6. Residual bedload transport: (a) bedload (sand) transport vectors calculated over the complete tidal cycle, showing a bedload convergent zone towards the bank crest (model results (®)).

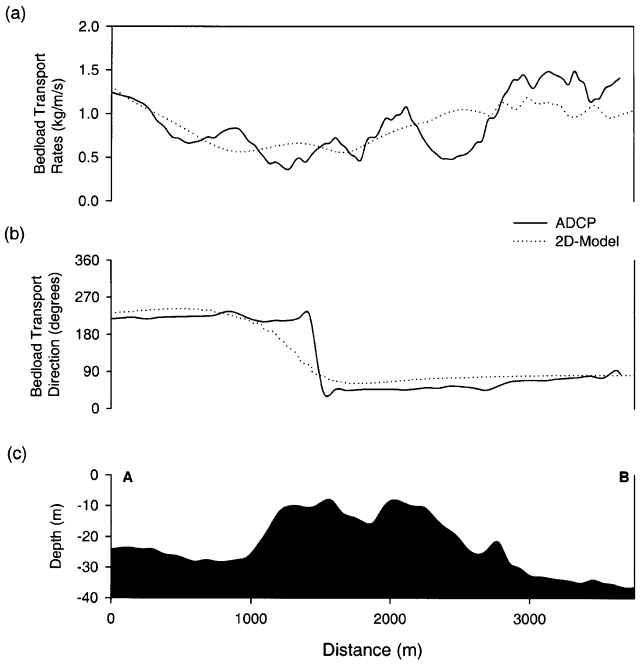

Fig. 7. Residual bedload transport rates computed along the Shambles Bank transect (defined in Fig. 1) showing a comparison between the rates derived from ADCP measurements (solid line) and 2D model (dotted line): (a) residual bedload transport rates showing a decrease in sediment transport rates towards the bank crest; (b) residual bedload transport direction showing sediment convergence towards the bank crest; and (c) topographic profile of the Shambles Bank along the survey transect (for location, see Fig. 1).

area, were found to lie at an ESE–WNW orientation (100°–280°); this placed them obliquely to the transect direction, at a 60° angle. The seabed at the time of maximum flood currents (1.35 m s^{-1} depth-averaged, see Fig. 2) is shown in Fig. 8a; the lee (steep) side of the sandwaves faced N–NE (10° from N). Such flood-dominated asymmetry was observed for another 3 h, following the maximum currents. With reversal in the tidal flow and the beginning of the ebb half-cycle, the side-scan sonar records show a pattern associated with ripple *cat-back* formations (van Veen, 1935; Berne et al., 1993); this is indicative of the initial erosion of the SSW crests (Fig. 8b). At maximum ebb currents (1.50 m s^{-1} depth-averaged, see Fig. 4), the lee side of the sandwaves was found to be orientated towards the S–SW (190° from N) (Fig. 8c). Towards the end of the tidal cycle, the ripple *cat-back* formations are again observed on the side-scan sonar record; they correspond with flow reversal from ebb- to flood-dominated currents.

4.4. Bedload transport and bedform dynamics

The time-series bedload transport rates, predicted using near-bed (ADCP) currents and a mean grain size of 1.1 mm, are plotted in Fig. 9, together with bedload transport direction, as inferred from the bedform

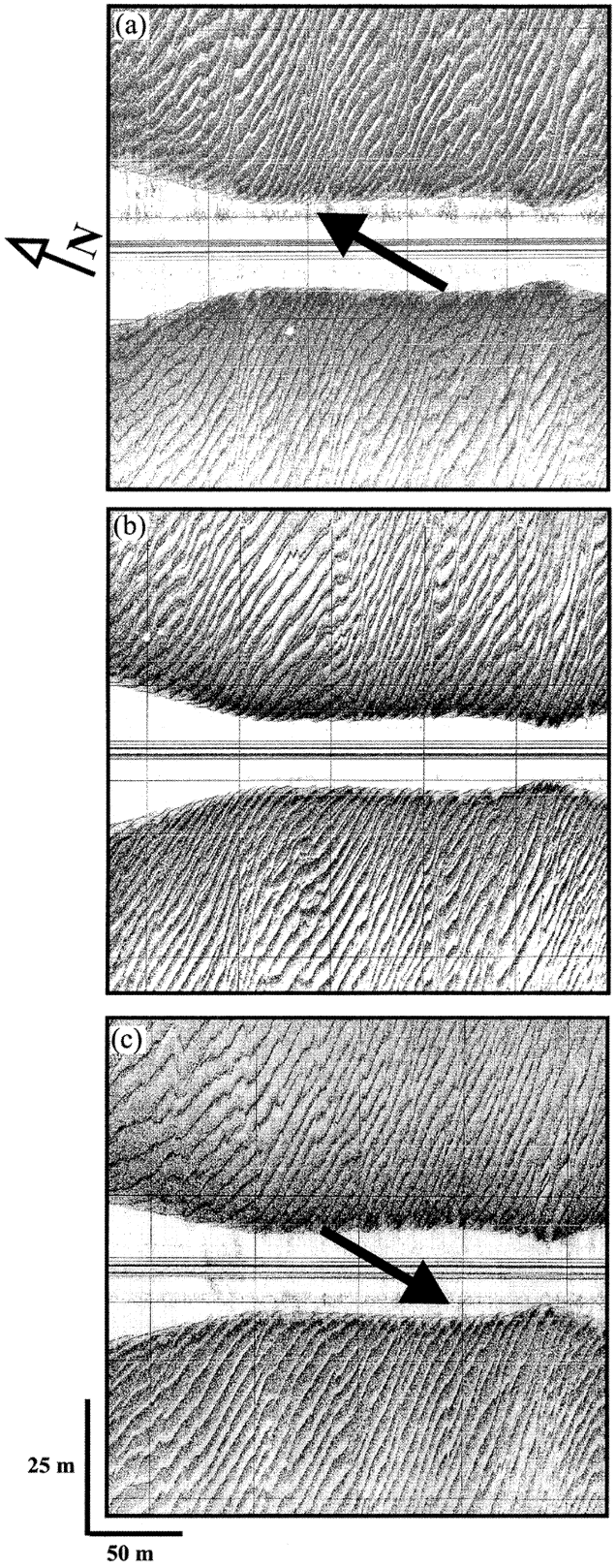

Fig. 8. Side-scan sonar images (for location, see Fig. 1) showing (light tone, associated with low backscatter): (a) small sandwaves, with flood-dominated asymmetry (indicated by the black arrow); (b) small sandwave *cat-back* formation, indicating erosion of the crest (during reversal); and (c) small sandwaves, with ebb-dominated asymmetry (indicated by the black arrow).

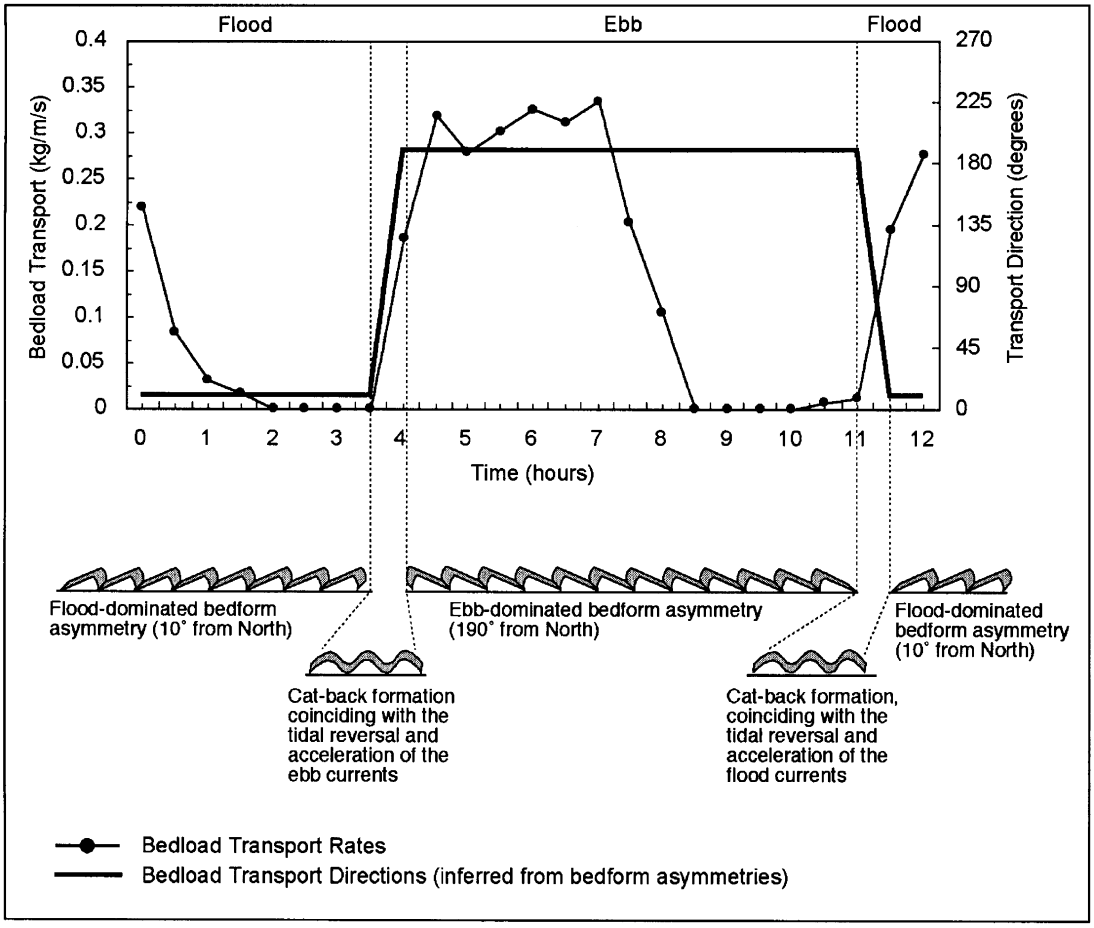

Fig. 9(a) Time-series of predicted bedload transport rates and directions calculated for the selected site associated with the sandwave reversal (Fig. 8; for location see Fig. 1). The transport rates were calculated using the near-bed currents measured by the ADCP, with a mean grain size of 1.1 mm. The bedload transport direction, as inferred by the bedform asymmetries, is also plotted. The observed bedform asymmetries representing the different stages of the tidal cycle are schematically represented at the bottom of the figure.

asymmetries, at the selected location (Fig. 1) along the survey transect. During the flood phase of the tide, bedload transport is reduced gradually to become insignificant 2 h before reversal of the tide. Over this period, the bedforms are flood-dominated, revealing a transport pathway towards the N–NE (10° from N). Within the first hour after the initiation of the tidal reversal, when bedload transport begins to increase, *cat-back* formations (near-bed currents $\sim$0.9 m s^{-1} and transport rates $\sim$0.18 kg m^{-1} s^{-1}) are observed; these coincide with the bedforms attempting to adjust to the changing hydrodynamic conditions. By the time the ebbing currents (near-bed $\sim$1 m s^{-1}) and bedload transport rates (0.32 kg m^{-1} s^{-1}) reach their maximum, the sandwaves have adjusted to the prevailing conditions and are completely reversed (indicating a transport pathway towards the S–SW, about 190° from the N). With the ebb phase of the tide drawing to an end (after about 6 h), transport rates are reduced. At the point of reversal, with subsequent acceleration of the flood currents, the *cat-back* formations were again detected; this was followed once again, by a reversal in the bedform asymmetry.

5. Discussion

The present investigation has examined the short-term dynamics of a sandbank (the Shambles Bank) in terms of water circulation, bedform mobility and bedload transport rates and pathways. The results suggest that two distinct tidally related sandbank maintenance processes are in operation, sequentially, throughout the tidal cycle. Hence, the tidally related sedimentary processes, that result in a bedload convergence towards the crest of the bank, appear to be influenced by: (a) the formation of headland-associated (Portland Bill) transient eddies during the flood phase of the tidal cycle and (b) the bottom-friction induced by the presence of the sandbank during the ebb phase of the tidal cycle. Distinct patterns of sediment transport were identified during the tidal cycle in relation to the hydrodynamically associated sandbank processes (as described above). Because of the

non-linearity of sediment transport to the prevailing flow conditions, instantaneous sand transport patterns do not necessarily follow the same transient pattern as that of the tidal flow.

During the flood phase of the tide, a zone of flow separation occurs at the tip of the headland with the strongest currents flowing towards the east (Fig. 2). In relation to the main axis of the Shambles Bank, orientated in an NE–SW direction (70°–250°), an anti-clockwise veering of the flood currents is induced. The result is the development of (anti-clockwise) transient eddies on the eastern side of the headland. Throughout the development of the transient eddies, sand transport is observed along the southern flank and towards the crest of the bank (Fig. 5a and b). Sand transport patterns during the flood phase of the tidal cycle can be examined by analysing the derived transport rates from the ADCP measurements (Fig. 10a). The along- and cross-bank sand transport components reveal that sand transport veers toward the bank crest (shown by the decrease in the along-bank component), followed by a significant decrease in sand transport rates; this can be interpreted as a zone of sand deposition/accumulation. Because of the development of transient eddies, sand transport rates reduce significantly along the northern flank (Fig. 10a), due to flow deceleration. During later stages of the flood tide, as the centre of the transient eddy migrates towards the bank, the transport rates reduce gradually; however, the transport pathway remains the same (as indicated by the bedform asymmetries).

The ebb currents are flowing towards the SW, approaching the northern flank of the bank obliquely, at an angle of 10°–15°; these set up an anti-clockwise veering towards the crest, followed by acceleration in the cross-bank velocity component (Fig. 4). As the flow leaves the sandbank, a clockwise veering of the currents occurs followed by an increase in the along-bank component. Thus, the observed water circulation pattern during the ebb phase of the tidal cycle, highlights the influence of bottom-friction induced by the presence of the sandbank, as described by the stability model proposed by Huthnance (1982b). This flow pattern results in an anti-clockwise sand transport veering towards the crest. Sand transport patterns during the ebb phase, derived from ADCP measurements (Fig. 10b), show clear evidence of sand transport veering towards the bank crest (shown by a decrease in the along-bank component), followed by an overall decrease in sand transport rates. As indicated previously for the flood phase of the tide, such a decrease in sand transport rates along the bank crest can be interpreted as a zone of sand deposition/accumulation. As the ebbing flow leaves the sandbank, a clockwise veering of sand transport, followed by an increase in transport rates, is observed along the southern flank. A conceptual model, summarising these results is shown in Fig. 11.

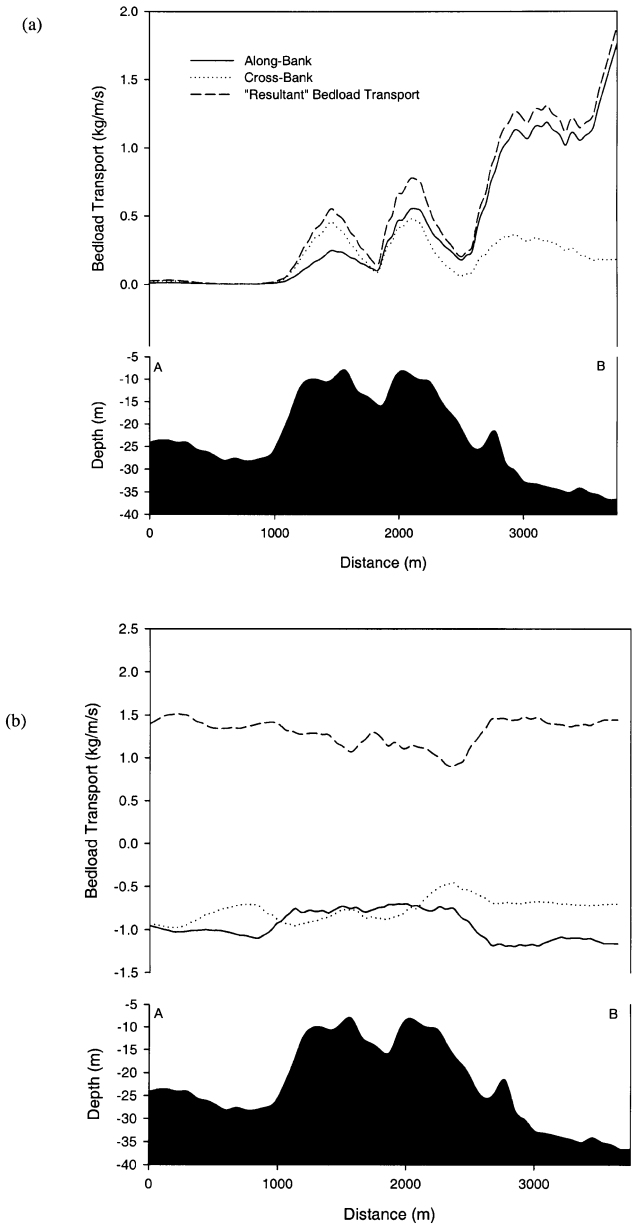

Fig. 10. Instantaneous sand transport rates (resultant, along and cross-bank components) across the Shambles Bank. Rates were derived from ADCP measurements, combined with the SEDTRANS model: (a) sand transport rates calculated during maximum flood currents; and (b) sand transport rates calculated during maximum ebb currents. For the location of the topographic profile of the Shambles Bank, see Fig. 1.

The presence of secondary flows in the plane normal to the mean current field, as indicated by the veering of the current direction with depth, was observed directly in the ADCP measurements and reached speeds of up to 0.20 m s^{-1} (10% of the maximum surface currents). These currents are comparable with those observed (5–15% of the streamwise flow) by Geyer (1993) around Gay Head (Massachusetts, USA) and those predicted (about 10% of the peak currents) by Heathershaw and Hammond (1980) for the Scarweather Sands (Bristol Channel, UK). Secondary flows are generated by the flow curvature; they

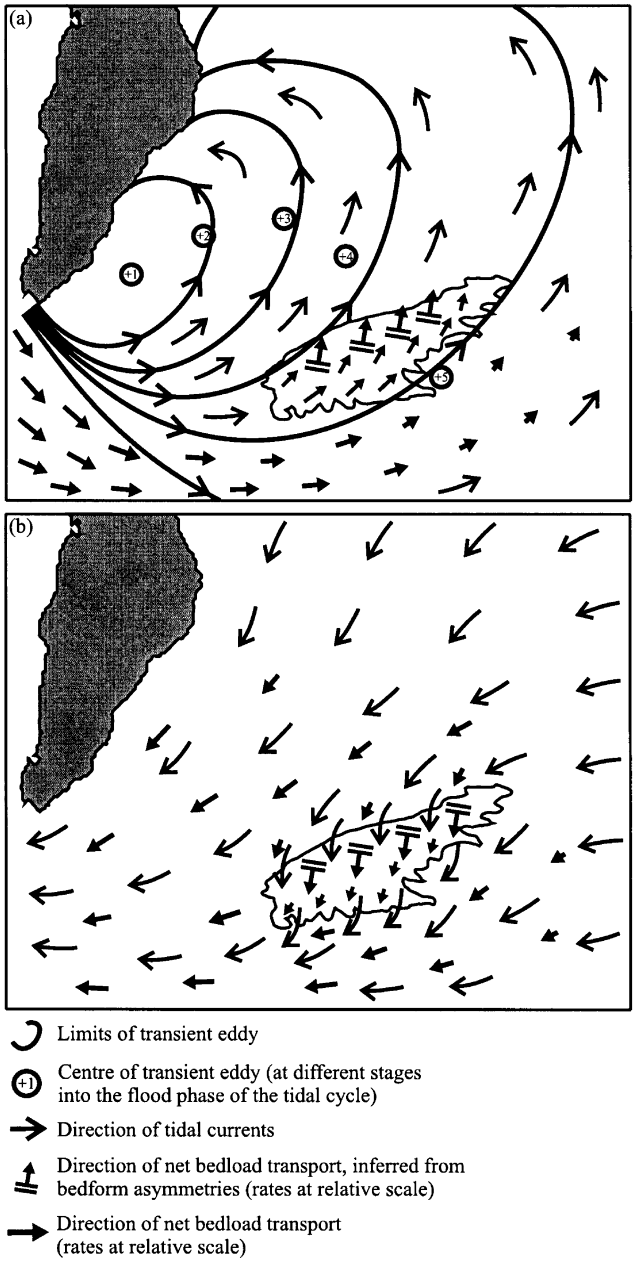

Fig. 11. A conceptual model of the tidally related maintenance processes, acting on a headland-associated sandbank: (a) the development of transient eddies, during the flood phase of the tidal cycle and (b) the effect of bottom-friction induced by the presence of the sandbank, during the ebb phase of the tidal cycle.

interact with the primary flow and can influence significantly its structure and affect the horizontal and vertical water-mass transport around a coastal headland (Geyer, 1993). In terms of sediment transport processes around a sandbank, the presence of such currents have been related to *helical cells* that would act as a mechanism to transport and concentrate sand along the crest of the banks (Houbolt, 1968; Heathershaw and Hammond, 1980). However, considering that the magnitude of such currents is only about 10% of the maximum primary flow, their capacity in transporting sediments appears to be minimal. Hence, secondary flows may have an indirect influence (related to the current veering) in sand transport processes around sandbanks.

The predicted bedload transport rates and directions, throughout the complete tidal cycle, indicate that the crest of the bank acts as a bedload convergence zone (see also Figs. 6 and 7). This has resulted from an anti-clockwise veering of the sand transport towards the crest, followed by a decrease in transport rates. This pattern has been observed elsewhere on the basis of geomorphological evidences and in situ measurements (Houbolt, 1968; Caston, 1972; Kenyon et al., 1981; Pattiaratchi and Collins, 1987; Lanckneus and de Moor, 1995; Collins et al., 1995; Williams et al., 2000). Such an interpretation differs conceptually from the residual circulation results, as it includes the non-linear dependence of sand transport.

In terms of the morphology of the Shambles Bank, a geophysical investigation has revealed the occurrence and distribution of very-large asymmetric sandwaves (Bastos et al., 2002); these show convergent sand transport towards the bank crest, corroborating the predicted net sediment transport patterns. The presence of superimposed small and medium sandwaves, forming usually an oblique angle (with crest directions at about 280°–100°) with the main bank axis and with the very-large sandwave crests (Fig. 8), indicate the veering of sand transport paths towards the bank crest. This provides evidence of the significance of the cross-bank velocity (transport) component. Such a pattern has been observed also on Type 1 sandbanks (or linear sand ridges) in the North Sea (Houbolt, 1968; Kenyon et al., 1981; McCave and Langhorne, 1982; Lanckneus and de Moor, 1995). The seabed time-series obtained over the Shambles Bank has revealed the complete reversal of small sandwaves, during the ebb-flood cycle (on spring tides), with an intermitting period (indicating the beginning of the reversal process) characterised by *cat-back* formations. The short-term reversal of small to medium sandwaves over sandbanks and shoals, has been described elsewhere (Hawkins and Sebbage, 1972; Boersma and Terwindt, 1981; Terwindt and Brouwer, 1986). Moreover, the reversal of large sandwaves over sandbanks has also been observed, however, in a medium- to long-term temporal scale (Berne et al., 1993; Lanckneus and de Moor, 1995). Hence, small and medium sandwaves can provide a good indication of short-term dynamic sediment transport processes over a sandbank.

In the case of headland-associated sandbanks, Pattiaratchi and Collins (1987) suggested previously that the maintenance process for the Scarweather Sands (Bristol Channel, UK) was the result of a combination of different possible mechanisms: the tidal stirring concept (Pingree, 1978); bottom-friction, induced by the sandbank (stability model, Huthnance, 1982a,b); and the

presence of helicoidal (secondary) flows (the spiral flow concept; Houbolt, 1968 and Heathershaw and Hammond, 1980). For the Shambles Bank, sand transport patterns derived from field measurements infer two different maintenance processes operating over the sandbank, during different stages of the tide (Fig. 10). The associated bedload transport investigations appear to indicate that the transient tidal eddy formation is the dominant process over the flood phase of the tide, whereas bottom-friction (induced by the presence of the sandbank) appears to explain better the maintenance process operating during the ebb phase of the cycle. During both phases of the tidal cycle, an overall decrease in sand transport rates was observed along the crest of the bank, suggesting a zone of sand deposition/accumulation. Although the presence of secondary flows was observed, their contribution to bedload transport is uncertain, as the magnitude of the vertical circulation of the flow was only some 10% of the surface peak tidal currents.

6. Conclusions

The tidally induced, short-term, sand transport pattern over the Shambles Banks is characterised by a sand convergent zone along the crest of the bank, followed by a decrease in sand transport rates. Although this derived pattern is similar to those described elsewhere, the evidence presented here seems to indicate towards the possibility of two different processes operating during the flood and ebb phases of the tidal cycle. During the flood phase of the tide, sand transport (directed towards the crest through the southern flank of the bank) appears to be controlled by the formation of transient eddies. During the ebb phase of the tide, bottom-friction induced by the presence of the bank seems to be the dominant process controlling sand transport (directed again towards the crest through the northern flank of the bank). Finally, although the results may have suggested that sand transport is controlled by different tidally related mechanisms, the overall net sand transport circulation pattern is related to: (a) deceleration in the along-bank component and (b) an increase in the cross-bank component (with a general decrease in flow, over the bank). This process was observed during both phases of the tidal cycle in the ADCP measurements and was corroborated by the orientation and mobility of the small sandwaves. Such process can provide a mechanism for the veering of sand transport towards the bank crest, together with the deposition of sedimentary material. As a recommendation for future research the use of a 3D hydrodynamic model, in combination with a detailed bathymetric grid, will offer certain advantages towards the investigation of processes relating to patterns of sand transport around sandbanks. A more accurate representation of the 3D structure of the flow in the vicinity of the sandbank, compared with the use of a 2D model, will be beneficial to the overall understanding of the sediment dynamic processes.

Acknowledgements

The first author (ACB) was supported, during the study, by a Scholarship awarded by the Conselho Nacional de Pesquisa (CNPq, Brazilian Government). Financial support for the fieldwork campaign and data acquisition was provided by SCOPAC (Standing Conference of Problems Associated to the Coastline, southern UK). The authors would like to thank: the Geological Survey of Canada, for providing the sediment transport model; H.R. Wallingford for providing the hydrodynamic model results; Mr John Davies (SOES), for his assistance in the field data collection; and Mrs K. Davis (SOES) for help in the preparation of Fig. 8. Thanks are also extended to the Editor (Dr E. Wolanski) and the three referees involved in the reviews for their constructive comments.

References

Ashley, G.M., 1990. Classification of large-scale subaqueous bedforms: a new look at an old problem. Journal of Sedimentary Petrology 60 (1), 160–172.

Bastos, A.C., Kenyon, N.H., Collins, M.B., 2002. Sedimentary processes, bedforms and facies, associated with a coastal headland: Portland Bill, southern UK. Marine Geology 187 (3–4), 235–258.

Belderson, R.H., Johnson, M.A., Kenyon, N.H., 1982. Bedforms. In: Stride, A.H. (Ed.), Offshore Tidal Sands: Processes and Deposits. Chapman and Hall, London, pp. 27–57.

Berne, S., Castaing, P., Le Drezen, E., Lericolas, G., 1993. Morphology, internal structure and reversal of asymmetry of large subtidal dunes in the entrance to Gironde Estuary (France). Journal of Sedimentary Research 65 (5), 780–793.

Berne, S., Trentesaux, A., Stolk, A., Missiaen, T., de Batist, M., 1994. Architecture and long term evolution of a tidal sandbank: the Middelkerke Bank (southern North Sea). Marine Geology 121, 57–72.

Boersma, J.R., Terwindt, J.H.J., 1981. Neap–spring tide sequences of intertidal shoal deposits in a mesotidal estuary. Sedimentology 28, 151–170.

Brampton, A., Evans, C.D.R., Velegrakis, A.F., 1998. South coast mobility study: west of the Isle of Wight. Construction Industry Research and Information Association (CIRIA) Report PR65. 201 pp.

Calvete, D., Walgreen, M., De Swart, H.E., Falques, A., 2001. A model for sand ridges on the shelf: effect of tidal and steady currents. Journal of Geophysical Research 106 (C5), 9311–9325.

Caston, V.N.D., 1972. Linear sandbanks in the southern North Sea. Sedimentology 18, 63–78.

Collins, M.B., Shimwell, S.J., Gao, S., Powell, H., Hewitson, C., Taylor, J.A., 1995. Water and sediment movement in the vicinity of linear sandbanks: the Norfolk Banks, southern North Sea. Marine Geology 123, 125–142.

De Vriend, H.J., 1990. Morphological processes in shallow tidal seas. In: Cheng, R.T. (Ed.), Residual Currents and Long Term Transport. Springer-Verlag, New York, pp. 276–301.

Dewez, S., Clabaut, P., Vicaire, O., Beck, C., Chamley, H., Augris, C., 1989. Transits sedimentaires resultants aux confins Manche-mer du Nord. Bulletin de la Societe Geologique de France 5, 1043–1053.

Dolan, R., Hayden, B., Felder, W., 1979. Shoreline periodicities and linear offshore shoals. Journal of Geology 87, 393–402.

Dyer, K.R., Huntley, D.A., 1999. The origin, classification and modelling of sandbanks and ridges. Continental Shelf Research 19, 1285–1330.

Ferentinos, G., Collins, M.B., 1980. Effects of shoreline irregularities on a rectilinear tidal current and their significance in sedimentation processes. Journal of Sedimentary Petrology 50 (4), 1081–1094.

Gadd, P.E., Lavelle, J.W., Swift, D.J., 1978. Estimate of sand transport on the New York shelf using near-bottom current meter observations. Journal of Sedimentary Petrology 48, 239–252.

Geyer, W.R., 1993. Three-dimensional tidal flow around headlands. Journal of Geophysical Research 98 (C1), 955–966.

Grochowski, N.T.L., Collins, M.B., Boxall, S.R., Salomon, J.C., 1993. Sediment transport predictions for the English Channel, using numerical models. Journal of Geological Society of London 150, 683–695.

Hawkins, A.B., Sebbage, M.J., 1972. The reversal of sand waves in the Bristol Channel. Marine Geology 12, M7–M9.

Heathershaw, A.D., Hammond, A.D.C., 1980. Secondary circulation near sandbanks and in coastal embayments. Deutsche Hydrographische Zeitschrift 33 (4), 135–151.

Hervouet, J.M., 1991. TELEMAC, a fully vectorised finite element software for shallow water equations. HE43/91-27, Electricite de France. 55 pp.

Houbolt, J.H.C., 1968. Recent sediments in the Southern Bight of the North Sea. Geologie Mijnb 47, 245–273.

Houthuy, R., Trentesaux, A., De Wolf, P., 1994. Storm influences on a tidal sandbank's surface (Middelkerke Bank, southern North Sea). Marine Geology 121, 23–41.

Hulscher, S.J.M., de Swart, H.E., de Vriend, H.J., 1993. The generation of offshore tidal sand banks and sand waves. Continental Shelf Research 13 (11), 1183–1204.

Hulscher, S.J.M.H., van den Brink, G.M., 2001. Comparison between predicted and observed sand waves and sand banks in the North Sea. Journal of Geophysical Research 106 (C5), 9327–9338.

Hulscher, S.J.M.H., 1996. Tide-induced large-scale regular bed form patterns in a three-dimensional shallow water model. Journal of Geophysical Research 101, 20727–20744.

Huthnance, J.M., 1982a. On one mechanism forming linear sandbanks. Estuarine, Coastal and Shelf Science 14, 79–99.

Huthnance, J.M., 1982b. On the formation of sandbanks of finite extent. Estuarine, Coastal and Shelf Science 15, 277–299.

Kenyon, N.H., Belderson, R.H., Stride, A.H., Johnson, M.A., 1981. Offshore tidal sandbanks as indicators of net sand transport and as potential deposits. In: Nio, S.D., Shuttenhelm, R.T.E., van Weering, T.C.E. (Eds.), Holocene Marine Sedimentation in the North Sea Basin 5. Blackwell Science, Oxford, pp. 257–268.

Lanckneus, J., de Moor, 1995. Bedforms on the Middelkerke Bank, southern North Sea. In: Flemming, B.W., Bartholoma, A. (Eds.), Tidal Signatures in Modern and Ancient Sediments. Blackwell Science, Oxford, pp. 33–51.

Li, M.Z., Amos, C.L., 1995. SEDTRANS92: a sediment transport model for continental shelves. Computers and Geosciences 21 (4), 533–554.

McCave, I.N., Langhorne, D.N., 1982. Sandwaves and sediment transport around the end of a tidal sand bank. Sedimentology 29, 95–110.

Off, T., 1963. Rhythmic linear sand bodies caused by tidal currents. Bulletin of the American Association of Petroleum Geologists 47, 324–341.

Paphitis, D., Collins, M.B., Nash, L.A., Wallbridge, S., 2002. Settling velocities and entrainment thresholds of biogenic sands (shell fragments) under unidirectional flow. Sedimentology 49, 211–225.

Pattiaratchi, C., Collins, M.B., 1987. Mechanisms for linear sandbank formation and maintenance in relation to dynamical oceanographic observations. Progress in Oceanography 19, 117–176.

Pingree, R.D., 1978. The formation of the Shambles and other banks by tidal stirring of the seas. Journal of the Marine Biological Association U K 58, 211–226.

Signell, R.P., Harris, C.K., 2000. Modeling sandbank formation around tidal headlands. In: Spaulding, M.L., Blumberg, A.F. (Eds.), Proceedings Sixth International Conference Estuarine and Coastal Modelling, New Orleans, LA, November 1999, ASCE Press, New Orleans, LA.

Smith, J.D., 1969. Geomorphology of a sand ridge. Journal of Geology 77, 39–55.

Swift, D.J., 1975. Tidal sand ridges and shoal-retreat massifs. Marine Geology 18, 105–134.

Tee, K., 1976. Tide-induced residual current, a 2-D nonlinear numerical tidal model. Journal of Marine Research 34, 603–628.

Terwindt, J.H.J., Brouwer, M.J.N., 1986. The behaviour of intertidal sandwaves during neap–spring tide cycles and the relevance for paleoflow reconstruction. Sedimentology 33, 1–31.

Tessier, B., Corbau, C., Chamley, H., Auffret, J.P., 1999. Internal structure of shoreface banks revealed by high-resolution seismic reflection in a macrotidal environment (Dunkerque Area, Northern France). Journal of Coastal Research 15 (3), 593–606.

Trowbridge, J.H., 1995. A mechanism for the formation and maintenance of shore-oblique sand ridges on storm-dominated shelves. Journal of Geophysical Research 100 (C8), 16071–16086.

van Veen, J., 1935. Sandwaves in the Southern North Sea. International Hydrology Review 12, 21–29.

Williams, J.J., MacDonald, N.J., O'Connor, B.A., Pan, S., 2000. Offshore sandbank dynamics. Journal of Marine Systems 24, 153–173.

Yalin, M.S., 1977. Mechanics of Sediment Transport. Pergamon Press, Oxford, 290 pp.